TIMP3 Overexpression in Macrophages Protects From Insulin Resistance, Adipose Inflammation, and Nonalcoholic Fatty Liver Disease in Mice

Rossella Menghini,[1] Viviana Casagrande,[1] Stefano Menini,[2] Arianna Marino,[1] Valeria Marzano,[1,3] Marta L. Hribal,[4] Paolo Gentileschi,[5] Davide Lauro,[1] Orazio Schillaci,[6,7] Giuseppe Pugliese,[2] Paolo Sbraccia,[1] Andrea Urbani,[1,3] Renato Lauro,[1] and Massimo Federici[1]

The tissue inhibitor of metalloproteinase (TIMP)3, a stromal protein that restrains the activity of proteases and receptors, is reduced in inflammatory metabolic disorders such as type 2 diabetes mellitus (T2DM) and atherosclerosis. We overexpressed *Timp3* in mouse macrophages (MacT3) to analyze its potential antidiabetic and antiatherosclerotic effects. Transgenic mice with myeloid cells targeting overexpression of TIMP3 were generated and fed a high-fat diet for 20 weeks. Physical and metabolic phenotypes were determined. Inflammatory markers, lipid accumulation, and insulin sensitivity were measured in white adipose tissue (WAT), liver, and skeletal muscle. In a model of insulin resistance, MacT3 mice were more glucose tolerant and insulin sensitive than wild-type mice in both in vitro and in vivo tests. Molecular and biochemical analyses revealed that increased expression of TIMP3 restrained metabolic inflammation and stress-related pathways, including Jun NH_2-terminal kinase and p38 kinase activation, in WAT and liver. TIMP3 overexpression in macrophages resulted in reduced activation of oxidative stress signals related to lipid peroxidation, protein carbonylation, and nitration in WAT and liver. Our data show that macrophage-specific overexpression of TIMP3 protects from metabolic inflammation and related metabolic disorders such as insulin resistance, glucose intolerance, and nonalcoholic steatohepatitis. ***Diabetes*** **61:454–462, 2012**

Obesity is a chronic disorder characterized by major metabolic complications, including insulin resistance and steatohepatitis, often coexisting in patients with type 2 diabetes mellitus (T2DM) (1–3). Recent studies suggest that low-grade inflammation might promote the onset of insulin resistance and hepatic steatosis (4,5). The triggers and the mechanisms provoking the accumulation of inflammatory cells and the release of cytokines within adipose tissue and liver are still undefined, although free fatty acids have been suggested to play a major part in this process (6). On the other hand, the modulation of inflammatory components within the adipose tissue, including monocytes/macrophages and T cells, has been shown to improve not only the obesity-induced inflammatory responses but also their metabolic complications in experimental models (7–9). Nevertheless, it has not been fully elucidated whether inflammation per se leads to the development of diabetes and which molecules and mechanisms might be involved.

We recently reported that deficiency of tissue inhibitor of metalloproteinase (TIMP)3 acts at the interface of inflammation and insulin resistance (10). TIMP3 is a secreted 24–27-kDa protein belonging to the family of TIMPs that binds to the extracellular matrix and inhibits metalloproteases such as matrix metalloproteinase-2/9 and sheddases such as tumor necrosis factor (TNF)-α converting enzyme (also known as ADAM17), participating in the modulation of inflammation, cellular migration, and proliferation (11,12). We and others have previously reported that the TIMP3/ADAM17 pathway is involved in the control of glucose homeostasis and adipose, hepatic, and vascular inflammation in both genetic and nutritional models of obesity in mice, as well as in patients with obesity-related T2DM and atherosclerosis (13–18). *Adam17*-null mice consistently show a hypermetabolic phenotype, and heterozygous *Adam17*$^{+/-}$ mice are protected from diet-induced obesity and inflammation (19,20). Furthermore, data from our and other laboratories have revealed that obesity is characterized by a deficiency of TIMP3 in white adipose tissue (WAT) and liver (14,21), suggesting that downregulation of TIMP3 in metabolic tissues may contribute to the deregulation of inflammatory pathways. To understand the extent to which TIMP3 could restrain the negative synergy between unchecked inflammation and nutrient overload, we generated a new mouse model with a cell-targeted overexpression of TIMP3 in myeloid cells (MacT3) in order to directly overexpress TIMP3 protein in key inflammatory sites (22). The aim of this strategy was to verify the hypothesis that TIMP3 could rescue the metabolic alterations associated with obesity.

RESEARCH DESIGN AND METHODS

Mouse model and metabolic analysis. The mouse *Timp3* gene was amplified by PCR with cDNA obtained from mouse muscle as a template. The gene was then cloned in a vector containing CD68 promoter/enhancer. For generation of transgenic mice, the linearized construct was microinjected into mouse pronuclei using standard methods as previously described (23,24). Offspring derived from the injections were genotyped by PCR and confirmed by Southern blotting. For hematopoietic cell lineage distribution, peripheral blood was collected from the tail vein and analyzed on a blood cell analyzer (Simply Cell; BPC BioSed, Rome, Italy) to determine cell counts.

For the diet-induced obesity model, mice were fed a high-fat diet (HFD) (60% of calories from fat; Research Diets, New Brunswick, NJ) or a normal diet (standard chow, 10% calories from fat, GLP; Mucedola s.r.l., Settimo Milanese,

From the [1]Department of Internal Medicine, University of Rome "Tor Vergata," Rome, Italy; the [2]Department of Clinical and Molecular Medicine, "Sapienza" University, Rome, Italy; the [3]Laboratory of Proteomics, EBRI/Santa Lucia Foundation, Rome, Italy; the [4]Department of Medical and Surgical Sciences, University of Magna Graecia, Catanzaro, Italy; the [5]Department of Surgery, University of Rome "Tor Vergata," Rome, Italy; the [6]Department of Diagnostic Imaging, University of Rome "Tor Vergata," Rome, Italy; and the [7]Istituto di Ricovero e Cura a Carattere Scientifico Neuromed, Pozzilli, Italy.

Corresponding author: Massimo Federici, federicm@uniroma2.it.

Received 9 May 2011 and accepted 21 November 2011.

DOI: 10.2337/db11-0613

This article contains Supplementary Data online at http://diabetes.diabetesjournals.org/lookup/suppl/doi:10.2337/db11-0613/-/DC1.

R.M. and V.C. contributed equally to this study.

Italy) for 20 weeks after weaning as indicated. Metabolic tests have previously been described (13). Hormones and adipokine levels were measured using commercial kits: insulin (Mercodia, Uppsala, Sweden) and adiponectin and leptin (R&D Systems, Minneapolis, MN). Aspartate aminotransferase and alanine aminotransferase levels were measured with a Modular P analyzer (Roche S.p.A, Monza, Italy).

Energy balance. Indirect calorimetry was performed using LabMaster (TSE Systems, Bad Homburg, Germany). All mice were acclimatized for 24 h before measurements were taken every 15 min for 24 h. V_{O_2} is expressed as milliliters of O_2 consumed per kilogram of body weight per minute. Carbon dioxide consumption (V_{CO_2}) is expressed as milliliters of CO_2 produced per kilogram of body weight per minute. The respiratory quotient is defined as V_{CO_2}/V_{O_2} and does not have any units. Activity was expressed by movement-induced beam interruptions per minute in the calorimeter. Daily food intake was monitored by weighing food hoppers.

Gene expression analysis. Total RNA was isolated from WAT, muscle, and liver, using TRIzol reagents (Invitrogen, Eugene, OR). A total of 2 μg total RNA was reverse transcribed into cDNA using the High Capacity cDNA Archive kit (Applied Biosystems, Foster City, CA). Quantitative real-time PCR was performed on individual samples using an ABI PRISM 7700 System and TaqMan reagents (Applied Biosystems). Each reaction was performed in triplicate using standard reaction conditions: 1 cycle at 50°C for 2 min, 1 cycle at 95°C for 10 min, and 40 cycles each at 95°C for 15 s and 60°C for 1 min. Calculations were performed via a comparative cycle threshold method (13).

Western blots. Western blots were performed on total tissue homogenates and macrophage extracts prepared as previously described (25). The following antibodies were used: TIMP3, actin, anti–phospho-Ser473 Akt and total Akt, anti–phospho-Thr183/Tyr185 Jun NH_2-terminal kinase (JNK) and total JNK, and anti–phosphoThr180/Tyr182 p38 and total p38 (Cell Signaling Technology, Danvers, MA). A representative image of eight mice per each group is shown.

ADAM17 activity and TNF-α levels. ADAM17 activity was determined as previously described (13). TNF-α levels were measured in cell medium using a commercial ELISA kit (R&D Systems) in accordance with the manufacturer's instructions.

Pancreata histological analysis and morphometry. Pancreata were fixed overnight in 4% paraformaldehyde and embedded in paraffin using standard techniques. Sections were stained with hematoxylin-eosin. Immunostaining for insulin was carried out with the Histomouse-SP kit (Zymed Laboratories, South San Francisco, California) according to the manufacturer's instructions. Six sections for each pancreas were imaged at ×20 magnification and quantified for surface areas. Areas corresponding to the β-cells were measured by dividing the area of insulin-positive immunoreactivity by whole pancreas area.

2,4-Dinitrophenyldrazine assay. Proteins were derivatized on carbonyl groups by 10 mmol/L 2,4-dinitrophenyldrazine (Sigma-Aldrich) in 2 N chloridric acid and were precipitated overnight with an ice-cold solution containing 50% ethanol, 25% methanol, and 25% acetone at –20°C. After four washes with the same ice-cold solution, the final pellet was dried at room temperature and redissolved in Laemmli sample buffer. After SDS-PAGE separation, proteins were electroblotted onto nitrocellulose membrane and immunodetection was performed using anti–2,4-dinitrophenyl keyhole limpet hemocyanin rabbit IgG (Molecular Probes, Eugene, OR) in order to evaluate carbonylated proteins. The immunoreactive bands were detected using goat anti-rabbit horseradish peroxidase–conjugated IgG (Bio-Rad Laboratories, Hercules, CA) and a chemiluminescence detection method (ECL; GE Healthcare, Buckinghamshire, U.K.).

Lipid peroxidation. Lipid peroxidation products were determined by thiobarbituric acid reactive substances (TBARSs) in protein extracts using colorimetric assay according to the manufacturer's instructions (LPO-586 Bioxytech; OXIS International, Foster City, CA).

In vivo positron emission tomography imaging. The positron emission tomography (PET) protocol included a localizer scan, a high-resolution (0.63 mm slice thickness) whole-body computed tomography study, and two 15-min whole-body PET acquisitions starting at 5 and 35 min after tracer administration. For assessment of fluorodeoxyglucose (FDG) distribution, transverse and dorsal slices were obtained, as well as whole-body three-dimensional maximum-intensity projections. Measurements of FDG distribution were obtained on dorsal planes using small regions of interest positioned on the brain, heart, liver, and limb. For each structure, measurements were obtained from four different slices and averaged. FDG uptake ratios for heart, liver, and forelimb were calculated using brain uptake as a reference structure that metabolizes glucose independent of insulin. Maximum standardized uptake values were calculated using a lean body mass algorithm.

Computed tomography scan. For in vivo scans, mice were anesthetized by 1% isoflurane inhalation and positioned with both legs fully extended. The entire torso of each mouse was scanned at an isotropic voxel size of 76 microns (45-kV, 133-μA, and 300-ms integration time) with a GE Explore Locus scanner (GE Heathcare Italia, Milano, Italy). Two-dimensional gray scale image slices were reconstructed into a three-dimensional tomographic image. Density values for soft tissue were calibrated from a five-point linear fit line using mixtures containing various ratios of two liquids, ranging from 0.78 mg/mL (100% ethanol; Sigma-Aldrich) to 1.26 mg/mL (100% glycerol; J.T. Baker, Phillipsburg, NJ). Density values for bone tissue were calibrated via a commercially available phantom containing hydroxyapatite rods of various densities (GE Healthcare).

Adipose tissue histological analysis. Histological procedures and antibodies have previously been described (13). The total number and cross-sectional areas of adipocytes were obtained by computer-assisted image analysis (Optimas 6.5; Bioscan, Edmunds, WA). Ten random fields per section were analyzed (size of field 0.78 mm^2), and values <100 μm^2 were automatically excluded from analysis because they were assumed to represent artifacts resulting from the image conversion process. The data were first averaged per section and then per animal. For the double immunofluorescence labeling study, sections were incubated with rat monoclonal anti-CD68 antibody and rabbit polyclonal anti-CD3 antibody (Abcam, Cambridge, MA). The stained sections were examined under a fluorescence microscope (Olympus BX51 equipped with Olympus C-3030 digital camera; Olympus, Tokyo, Japan).

Vascular density. WAT sections ($n = 8$) immunolabeled with the polyclonal goat anti-mouse CD31 antibody (PECAM-1; Santa Cruz Biotechnology, Santa Cruz, CA) were viewed at ×250. Twenty random fields per section were analyzed (size of field 0.125 mm^2). Images were converted in a binary format, and the number of vessels per field was counted and expressed as number of vessels per millimeter squared. Average blood vessel size was calculated by dividing the total stained area by the number of vessels.

Histology and quantification of liver lesions. Histological procedures have previously been described (14). F4/80, N^{ε}-(carboxymethyl)lysine (CML), and nitroTyr immunostaining were performed using antibodies (Abcam), following the manufacturer's instructions.

Isolation of adipocytes and stromal vascular fraction from WAT. To determine the relative expression of TIMP3 in adipocytes and stromal vascular fraction (SVF), WAT was subjected to collagenase digestion (1 mg/mL collagenase type 1; Sigma-Aldrich) in Krebs-Ringer buffer, with shaking at 150 rpm for 30 min at 37°C. After digestion, adipocytes were allowed to separate by flotation and the infranatant solution was centrifuged for 5 min at 300*g* to pellet the SVF. The adipocyte fraction was washed three times with the Krebs-Ringer buffer. Subsequently, RNA was isolated from adipocytes and the SVF fractions and analyzed by real time PCR. The profile of adiponectin mRNA expression provides evidence of the purity of the fraction preparations.

Isolation of hepatocytes and nonparenchymal cells from liver. Mice were anesthetized, and liver tissues were perfused in situ via the superior vena cava with a perfusion buffer (1× Hanks' balanced salt solution), followed by a digestion buffer (1× Hanks' balanced salt solution, supplemented with 0.05% collagenase [Type IV; Sigma Chemical, St. Louis, MO], 1.25 mmol/L $CaCl_2$, 4 mmol/L $MgSO_4$, and 10 mmol/L HEPES). The resulting cell suspension was filtered through a sterile 100-μm nylon mesh and centrifuged at 50*g* to selectively sediment hepatocytes from nonparenchymal cells (NPCs). The pellet of hepatocytes was resuspended and subsequently washed two more times at 50*g*. The NPCs in the first and second supernatants from the low-speed centrifugations were pelleted by high-speed centrifugation (1,300*g*), followed by resuspension in a small volume before isopycnic sedimentation in Percoll as previously described (26). Cell viability (>90%) was determined by trypan blue exclusion. The profile of albumin mRNA expression provides evidence for the purity of the fraction preparations.

Statistical analysis. Results of the experimental studies are expressed as means ± SD. Statistical analyses were performed using the one-way ANOVA or unpaired Student *t* test as indicated. Values of $P < 0.05$ were considered statistically significant.

RESULTS

Metabolic effect of diet-induced obesity on MacT3. We generated transgenic mice (MacT3) overexpressing *TIMP3* under the control of the monocyte/macrophage lineage-specific promoter CD68 in order to increase TIMP3 expression directly in metabolic tissues where myeloid cells are gradually recruited during obesity (22). Three positive founder lines, which gave germ line transmission, were expanded to establish the MacT3 transgenic colonies (data not shown). Because the overexpression of TIMP3 was comparable in the three lines and they showed similar features after a preliminary characterization, we used one of them for our studies. MacT3 mice fed a normal diet did not differ from wild-type (WT) littermates in terms of fasting and fed glucose insulin levels, glucose and

insulin tolerance, adiponectin, or leptin secretion (Supplementary Fig. 1*A–F*, available in the Supplementary Data).

For evaluation of the role of TIMP3 overexpression in the development of obesity, MacT3 and WT mice were fed an HFD for 20 weeks. MacT3 mice on an HFD did not show significant differences in white blood cell lineages or monocyte counts compared with WT littermates (Supplementary Fig. 2*A*). MacT3 mice did not differ in weight from WT mice while consuming the HFD (Fig. 1*A*) but showed improved fasting and fed glucose and insulin levels (Fig. 1*B*). Similarly, MacT3 mice showed improved glucose tolerance and insulin sensitivity compared with WT mice, as assessed by the intraperitoneal glucose tolerance test and intraperitoneal insulin tolerance test (Fig. 1*C*). In contrast, we did not observe any differences in glucose-stimulated insulin secretion, pancreatic islet numbers, or gross morphology in MacT3 mice compared with WT littermates fed an HFD (Supplementary Fig. 2*B–E*). Levels of adiponectin, transaminases, TNF-α, and interleukin (IL)-6 were improved in MacT3 mice compared with WT mice (Fig. 1*D*). Indirect calorimetry showed that MacT3 mice exhibited a slight significant increase in V_{O_2} and V_{CO_2}, activities, and food intake (Fig. 1*E* and *F*). To investigate whether the improvement in glucose homeostasis was due, at least in part, to an increase in glucose transport, we conducted a PET scan to directly measure FDG uptake after insulin infusion in both anterior and posterior legs, and we observed that the standardized uptake value was statistically higher in MacT3 mice compared with WT mice (Fig. 2*A*). MacT3 mice also showed an increased insulin-induced phosphorylation of Ser473 Akt, which is a major regulator of glucose uptake in muscle (Fig. 2*B*).

Effect of diet-induced obesity on adiposity in MacT3. To evaluate how an HFD impacts adipose tissue morphology and functions in MacT3 and WT mice, we analyzed adipose tissue depots in vivo through computed tomography scans, which revealed that MacT3 mice had a slightly decreased visceral adipose tissue fraction, despite a similar overall adiposity (Fig. 3*A*). Epididymal and perirenal fat pads were also smaller in MacT3 mice (Fig. 3*B* and

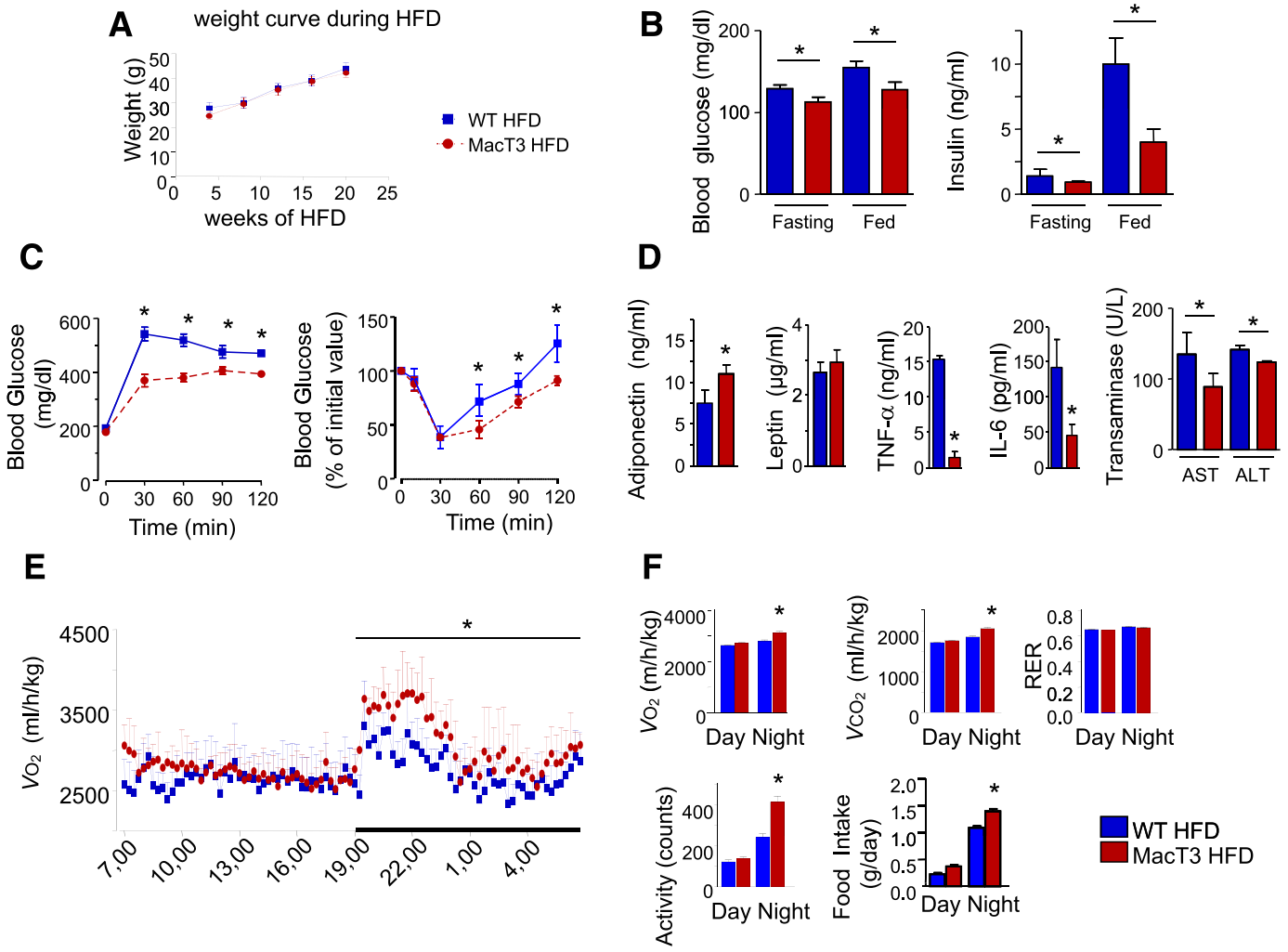

FIG. 1. MacT3 mice are protected against HFD-induced insulin resistance. WT and MacT3 mice were fed an HFD for 20 weeks. *A*: Body weight curve during HFD (n = 9 per group). *B*: Fasting and fed glucose and insulin levels (n = 9 per group; *P < 0.05, Student t test). *C*: Intraperitoneal glucose tolerance test and intraperitoneal insulin tolerance test (n = 9 per group; *P < 0.05, one-way ANOVA). *D*: Adiponectin, leptin, TNF-α, IL-6, and transaminase levels (n = 9 per group; *P < 0.05, Student t test. Data are means ± SD). *E*: Vo_2 in free-fed MacT3 mice over a period of 24 h (line chart) compared with Vo_2 in WT mice after 20 weeks of HFD. *F*: Mean 24-h values for Vo_2, Vco_2, respiratory quotient (RER), locomotor activity, and food intake. (*E* and *F*: n = 6 per group. Student t test, *P < 0.05 for MacT3 HFD vs. WT HFD mice. Data are means ± SD.)

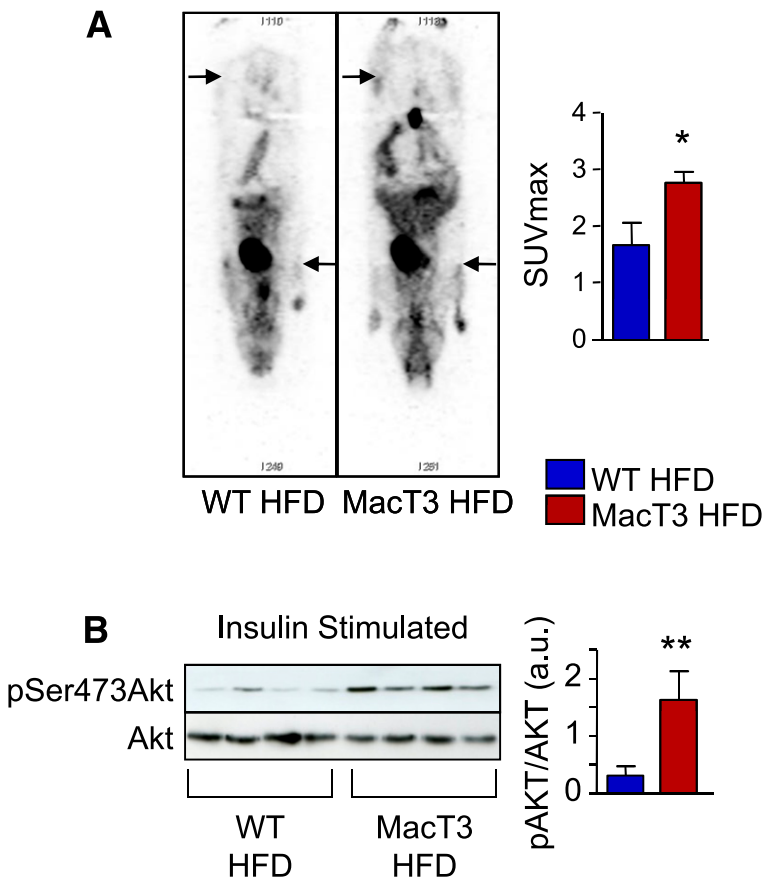

FIG. 2. MacT3 mice show improved insulin-stimulated glucose transport in vivo. *A*: Anterior images from the FDG PET scans of WT and MacT3 mice fed an HFD for 20 weeks. Arrows indicate sites with different glucose uptake in forelimbs and hind limbs. Maximum standardized uptake values (SUV_{max}) indicating an increased glucose uptake in MacT3 vs. WT mice. (n = 5 per group; *P < 0.05, Student t test. Data are means ± SD.) *B*: Skeletal muscle tissue from overnight-fasted WT and MacT3 mice fed an HFD for 20 weeks was dissected 5 min after insulin injection, and Akt phosphorylation (p) was analyzed by Western blot. (n = 8 per group; **P < 0.01, Student t test. Data are means ± SD.) A representative image of four mice per group is shown. a.u., arbitrary unit. (A high-quality color representation of this figure is available in the online issue.)

Supplementary Fig. 3*A*). WAT from MacT3 mice showed significantly increased TIMP3, both at mRNA and protein levels, and decreased ADAM17 activity (Fig. 3*C*). By analyzing isolated tissue fractions separately, we observed that expression of TIMP3 in adipocyte is significantly lower than in SVF in WT mice (Fig. 3*D*). In addition, TIMP3 level was further increased in SVF obtained from WAT of MacT3 mice compared with WT. Adiponectin mRNA expression was analyzed to confirm the purity of the two different fractions (Fig. 3*D*).

Histological analysis of HFD WAT sections showed a higher density of smaller adipocytes (Fig. 3*E* and Supplementary Fig. 3*B*). The insulin-sensitizing and anti-inflammatory hormone adiponectin, and oxidative stress markers such as TBARSs and the presence of protein carbonylation (2,4-dinitrophenyldrazine), was reduced in MacT3 mice compared with levels in WT mice (Fig. 3*F* and Supplementary Fig. 3*C* and *D*). Immunohistological analyses of inflammatory markers for macrophages (F4/80), T cells (CD3), and capillary density were conducted by CD31 staining and revealed a lower number of tissue macrophages and T cells and slightly reduced adipose tissue vascularization in MacT3 mice compared with WT mice (Fig. 4*A*). Analysis using immunofluorescence microscopy confirmed that CD68 and CD3 signals did not colocalize (Supplementary Fig. 4). These results were also supported by the lower mRNA expression of inflammatory markers (Fig. 4*B*) observed in MacT3 mice. MacT3 mice showed reduced activation of p38 and JNK (Fig. 4*C*), which allowed for increased phosphorylation of Akt kinase, the mediator of insulin metabolic effects, both in the fed state and after insulin stimulation (Fig. 4*D*).

Effect of diet-induced obesity on hepatic steatosis in MacT3. We recently observed that TIMP3 deficiency led to steatohepatitis under an HFD regimen (14). In contrast, under the same conditions MacT3 mice showed significantly reduced liver weights (Fig. 5*A*), higher levels of TIMP3 expression, and reduced ADAM17 activity (Fig. 5*B–D*). In addition, analysis of isolated hepatic cells (hepatocytes and NPCs) showed that TIMP3 mRNA was significantly overexpressed in nonparenchymal cells (which include Kupffer cells) from MacT3 mouse livers compared with expression in WT mouse livers (Fig. 5*E*). Albumin mRNA expression was analyzed in order to confirm the purity of the two different fractions (Fig. 5*E*).

Histological analysis revealed that obesity in livers from WT mice induced a macrovesicular steatosis similar to the grade-2 stage in humans and characterized by features such as ballooning degeneration; in contrast, MacT3 mouse livers were less steatotic (between grade 0 and grade 1) (Fig. 5*F*). Compared with WT mice, MacT3 mice revealed significantly reduced F4/80 staining and reduced oxidative stress, as suggested by markers such as N^{ε}-CML and nitroTyr staining (Fig. 5*F*). Analysis of TBARS levels in

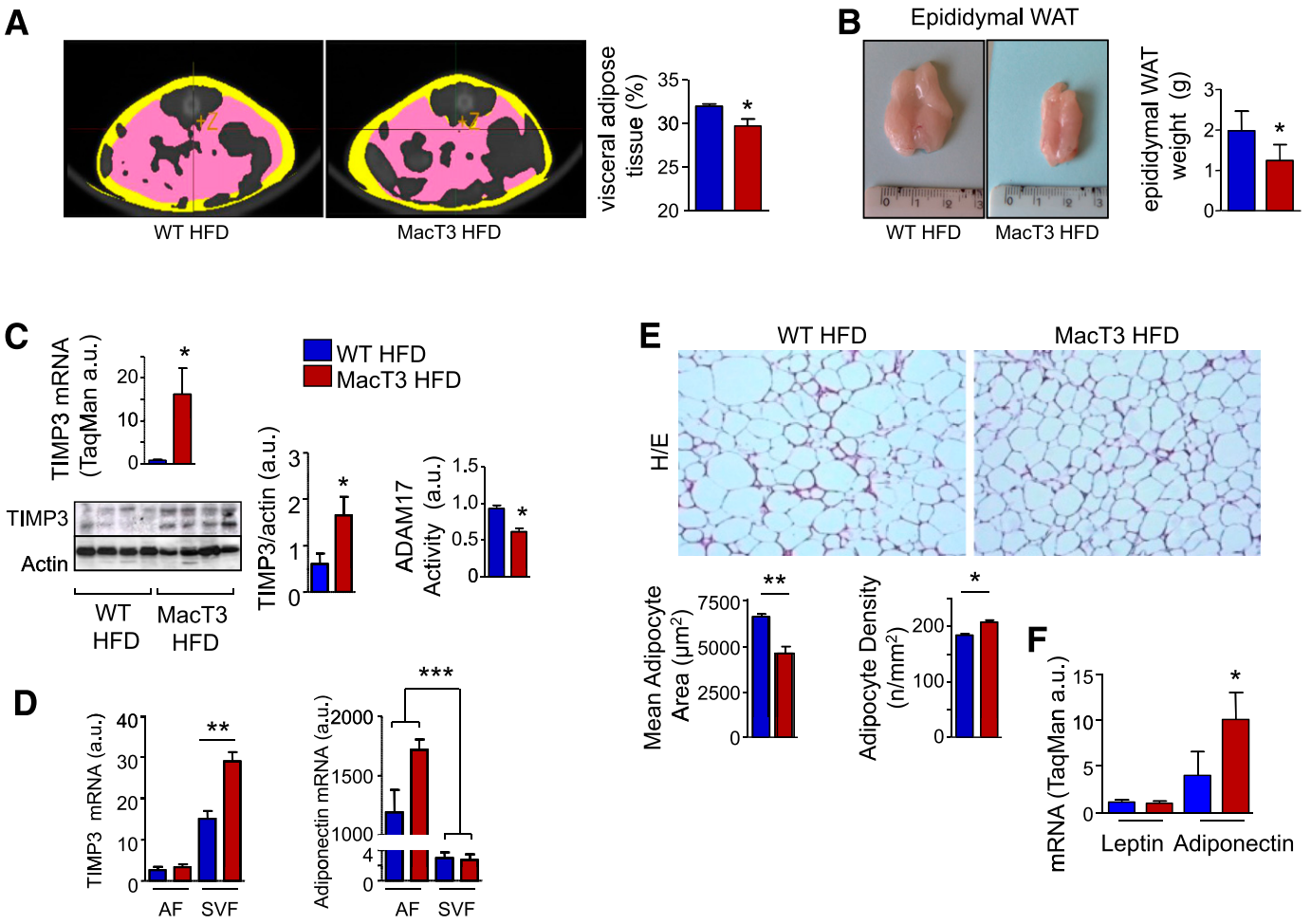

FIG. 3. MacT3 mice are protected against HFD-induced changes in adipose tissue. *A*: Representative computed tomography scan section indicating a decreased visceral adipose tissue fraction in MacT3 vs. WT mice fed an HFD for 20 weeks, confirmed by visceral adipose tissue quantification. (n = 4 per group; *P < 0.05, Student t test. Data are means ± SD.) *B*: Epididymal fat pads were harvested and weighed. (n = 5 per group; *P < 0.05, Student t test. Data are means ± SD.) *C*: TIMP3 mRNA and protein levels were increased and ADAM17 activity was reduced in adipose tissue of MacT3 mice fed an HFD compared with WT mice. A representative image of four mice per group is shown. (n = 8 per group; *P < 0.05, Student t test. Data are means ± SD.) *D*: TIMP3 and adiponectin (considered adipocyte markers) and mRNA expression in mature adipocytes (AFs) and SVF. (n = 5 per group; **P < 0.01 and ***P < 0.001, Student t test. Data are means ± SD.) *E*: Representative sections of adipose tissue stained with hematoxylin-eosin (H/E) showing an increased adipocyte density and a reduction in mean adipocyte area in MacT3 mice vs. WT mice. (n = 5 per group; **P < 0.01 and *P < 0.05, Student t test. Data are means ± SD.) *F*: WAT expression of leptin and adiponectin mRNA. Expression of mRNA was determined by real-time PCR and normalized to 18S RNA. (n = 5 per group; *P < 0.05, Student t test. Data are means ± SD.) a.u., arbitrary unit. (A high-quality digital representation of this figure is available in the online issue.)

liver homogenates confirmed reduced oxidative stress in MacT3 mice compared with WT mice (Fig. 6*A*). mRNA expression levels of oxidative stress genes (catalase, *SOD2*, *Gp47*, and *GP67*), and inflammatory (suppressor of cytokine signaling 3 and IL-6) and anti-inflammatory (IL-10) markers supported the histological evidence for reduced inflammation in the livers of MacT3 mice (Fig. 6*B*). As in adipose tissue, MacT3 mouse livers exhibited significantly lower activation of the stress kinase JNK and improved phosphorylation of Ser473 Akt both in the fed state and upon insulin stimulation (Fig. 6*C*).

DISCUSSION

Visceral obesity and the consequent low-grade inflammatory state are major determinants for the onset of insulin resistance and its metabolic sequels, T2DM and nonalcoholic fatty liver disease (NAFLD) (1,27). In this study, we have shown that a transgenic approach aimed to increase the levels of TIMP3 at the sites of metabolic inflammation is sufficient for containing the development of insulin resistance and NAFLD in vivo.

In the context of diet-induced obesity, TIMP3 improved insulin sensitivity and systemic glucose uptake in vivo. Although the overexpression of TIMP3 did not affect body weight, it was involved in the adipose tissue architecture. In fact, at the microscopic level the adipose tissue architecture in MacT3 mice was characterized by the presence of small adipocytes of higher density, suggesting an increase in metabolic activity (28). At the molecular level, TIMP3 overexpression resulted in a continued secretion of adiponectin, an anti-inflammatory and insulin-sensitizer hormone known to positively affect glucose and lipid metabolism, as well as liver inflammation (29,30). This was accompanied by a reduced inflammatory infiltrate and decreased IL-6 expression and secretion in vivo. Analysis of signaling readouts showed that in MacT3 mice, the activation of the insulin receptor pathway was preserved, to some extent, through reduction of the negative effect produced by stress kinases such as JNK and p38. Furthermore, computed

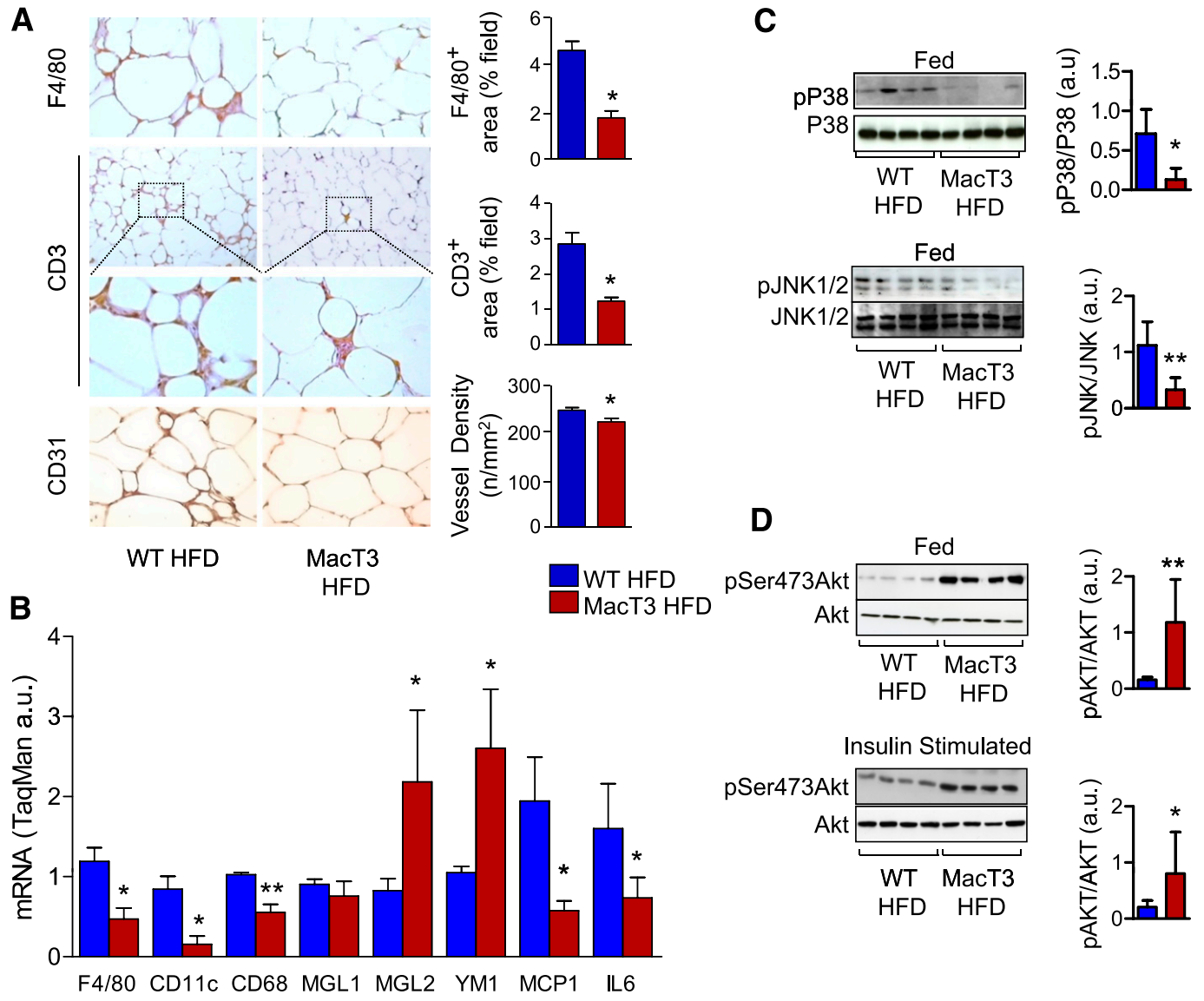

FIG. 4. Protective effect of transgenic expression of TIMP3 in macrophages on inflammation in WAT. *A*: Representative sections of WAT from WT and MacT3 mice fed an HFD for 20 weeks stained with F4/80, CD3, and CD31, revealing a reduction in macrophage and T-cell infiltration and in vessel density. (n = 5 mice per group; *P < 0.05, Student t test. Data are means ± SD.) *B*: WAT expression of genes involved in inflammation. Expression of mRNA was determined by real-time PCR and normalized to 18S RNA. (n = 5 per group; *P < 0.05 and **P < 0.01, Student t test. Data are means ± SD.) *C*: WAT from WT and MacT3 mice fed an HFD for 20 weeks was lysed and analyzed for phosphorylation of JNK and p38. *D*: WAT from WT and MacT3 mice fed an HFD for 20 weeks was lysed and analyzed for phosphorylation of Akt by Western blot (*upper panel*). Adipose tissue from overnight-fasted WT and MacT3 mice fed an HFD for 20 weeks was dissected 5 min after insulin injection; insulin-stimulated Akt phosphorylation (p) was analyzed by Western blot (*lower panel*). (*C* and *D*: For all Western blots, n = 8 per group; a representative image of four mice per group is shown. *P < 0.05 and **P < 0.01, Student t test. Data are means ± SD.) a.u., arbitrary unit. (A high-quality digital representation of this figure is available in the online issue.)

tomography scan and histological analyses revealed a reduction of the visceral adipose tissue fraction and microvessel density in MacT3 mice. Previous studies have shown that TIMP3 acts to stabilize vessels during angiogenesis and limits the development of an uncontrolled angiogenic response (31). Because antiangiogenic factors such as angiostatin demonstrated activity against obesity and its complications (32), we can conjecture that part of the TIMP3 effect on systemic metabolism may be due to its ability to stabilize the vessels inside adipose tissue. Therefore, it is possible that the action of TIMP3 on adipose tissue is sufficient for maintenance of metabolic control, thus avoiding the deterioration of liver metabolism, which is a central check point for both lipoprotein synthesis and the release of systemic inflammatory factors, such as IL-6. The current study showed that in mice fed a regular diet, TIMP3 was physiologically more expressed in the SVC fraction than in mature adipocytes, suggesting that the effect of TIMP3 on adipocytes may depend on the complex dynamics of inflammatory cells within the expanding adipose tissue during obesity. Still controversial is whether TIMP3 is involved in regulation of adipogenesis. In fact, some authors have suggested that TIMP3 might limit adipogenesis (21,33), while others have suggested that TIMP3 could favor adipogenesis via the limitation of the TNF-α converting enzyme–dependent shedding of Pref-1, a molecule that, when released from the membrane, is known to block the differentiation of the preadipocyte cell (34).

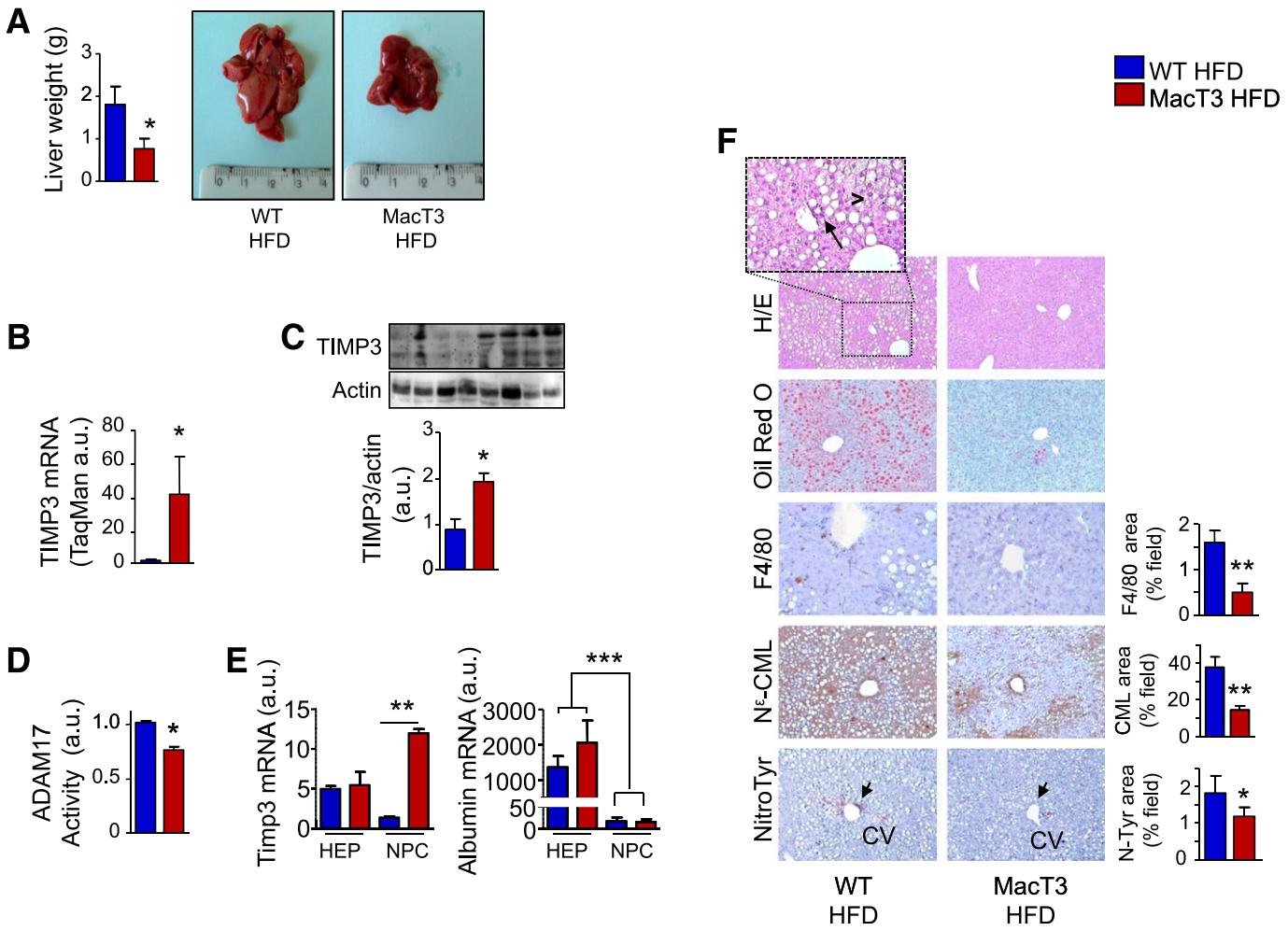

FIG. 5. Reduced hepatic steatosis in HFD-fed MacT3 mice. *A*: Livers of MacT3 and WT mice fed an HFD for 20 weeks were harvested and weighed. Results are expressed in grams. (n = 10 per group; *P < 0.05, Student t test. Data are means ± SD.) *B*: TIMP3 mRNA. *C* and *D*: TIMP3 protein levels (*C*) and ADAM17 activity (*D*) in livers of MacT3 mice compared with WT mice. (n = 8 per group; *P < 0.05, Student t test. Data are means ± SD.) *E*: TIMP3 and albumin (hepatocyte [HEP] marker) mRNA expression in purified hepatocytes and NPCs from MacT3 and WT mouse livers. (n = 5 per group; **P < 0.01 and ***P < 0.001, Student t test. Data are means ± SD). *F*: Representative sections of liver stained with hematoxylin-eosin (H/E), Oil Red O, F4/80, CML, or nitroTyr (N-Tyr). Arrow indicates a lipogranuloma in WT mice. CV, central vein. (n = 5 per group; **P < 0.01 and *P < 0.05, Student t test. Data are means ± SD.) a.u., arbitrary unit. (A high-quality digital representation of this figure is available in the online issue.)

Although our data support a major direct effect of TIMP3 in adipose tissue, we cannot exclude the possibility that the effects of TIMP3 on the liver parenchyma may also be involved in the MacT3 phenotype. In fact, it has been suggested that proinflammatory macrophages in the liver are characterized by reduced TIMP3 expression (35). We observed that hepatocytes expressed more TIMP3 than did cells in the nonparenchymal fraction. In MacT3 mice, we obtained a specific increase of TIMP3 in the fraction containing Kupffer and hepatic stellate cells, suggesting that the effect in the liver is independent of the cellular source, which is reasonable given that TIMP3 is released outside the cells and acts in the extracellular space.

Recently, it has been suggested that loss of TIMP3 could cooperate with epidermal growth factor receptor activation to dictate the resistance to Fas-induced apoptosis and hepatitis (36). The counterintuitive effect of apoptosis prevention is the unchecked activation of proliferative signals mediated by release of epidermal growth factor receptor ligands and TNF-α shedding, both of which are dependent on ADAM17. Therefore, while loss of TIMP3 could protect from acute insults to the liver, it may paradoxically promote hepatic inflammation and fibrosis, especially in synergy with nutrient overload (13,14). Whether the TIMP3/Fas connection is relevant for transition from fatty liver disease to steatohepatitis requires further studies, although Fas has been demonstrated to be relevant to NAFLD via its interaction with Met (37), and Met signaling may be affected by metalloprotease regulation (38).

Previous studies have shown individual effects of TIMPs on separate components of the metabolic syndrome or its complications, such as insulin resistance and obesity (13,39–44). However, among TIMPs only TIMP3 was found to be reduced in the adipose tissue of experimental models of obesity and insulin resistance when genes regulating matrix biology were analyzed (44).

Our study has clear strengths and limitations. In fact, our approach was designed to test the effect of TIMP3 at the site of metabolic inflammation independent of the physiological cellular sources. The coupling of TIMP3 to the CD68 promoter allowed us to test the effect of TIMP3 in a time-restrained manner because the transgenic TIMP3 is transcribed and released only when the CD68 promoter is activated. Therefore, it is intriguing to hypothesize that

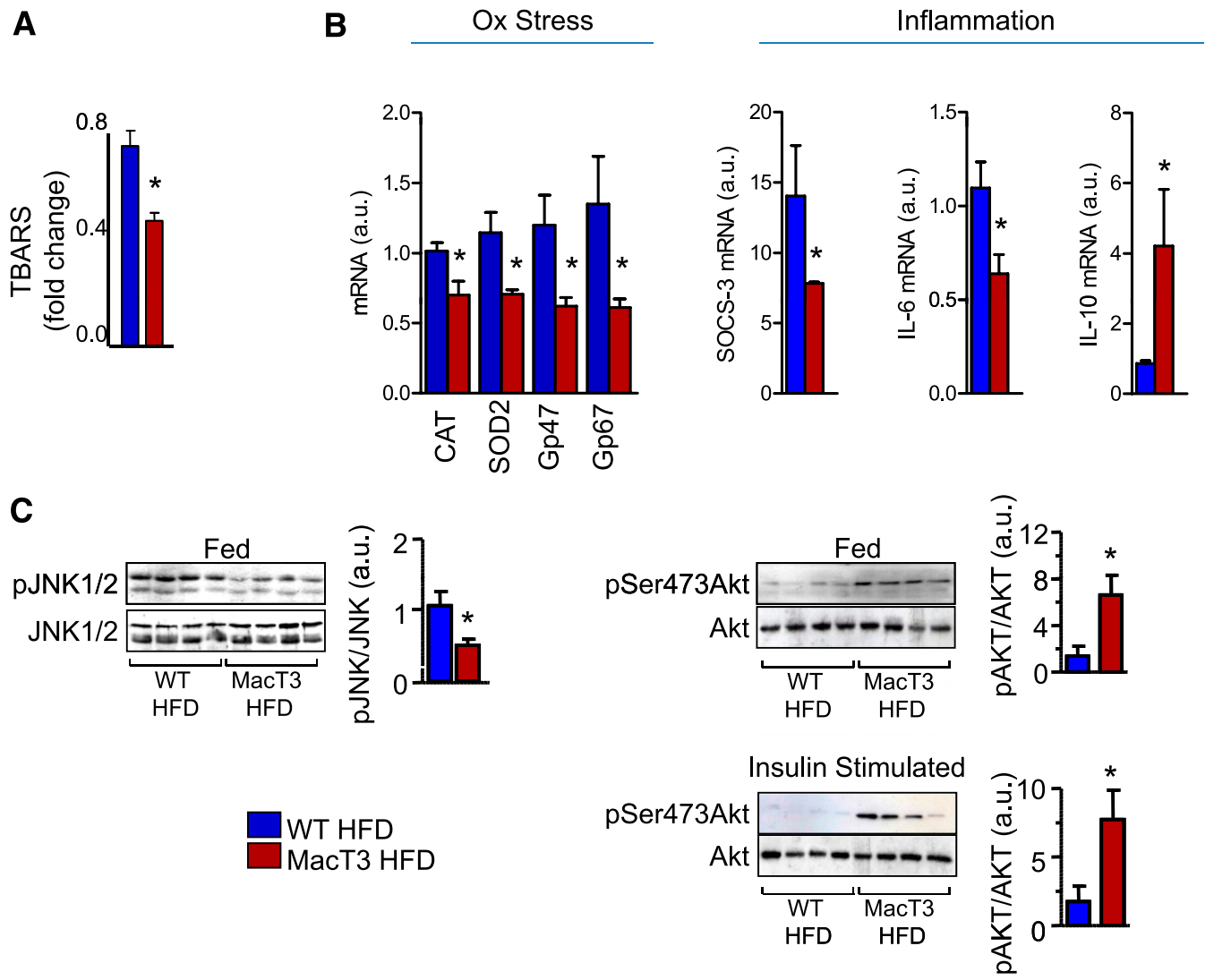

FIG. 6. Reduced hepatic oxidative (Ox) stress and improved insulin signaling in HFD-fed MacT3 mice. *A*: TBARS assay detecting lipid peroxidation products (fold change). (n = 5 per group; *P < 0.05, Student t test. Data are means ± SD.) *B*: mRNA expression of indicated markers in liver tissue of WT and MacT3 mice was analyzed by real-time PCR, expressed relative to WT, and normalized to expression of 18S. CAT, catalase. (n = 5 per group; *P < 0.05, Student t test. Data are means ± SD). *C*: Livers from WT and MacT3 mice fed an HFD for 20 weeks were lysed and analyzed for phosphorylation (p) of Akt and JNK by Western blot. For insulin-stimulated Akt phosphorylation, livers from overnight-fasted mice were dissected 5 min after insulin injection and analyzed by Western blot. (n = 8 per group. A representative image of four mice per group is shown. *P < 0.05, Student t test. Data are means ± SD.) a.u., arbitrary unit. (A high-quality color representation of this figure is available in the online issue.)

TIMP3 could restrain the inflammatory phenotype of a macrophage in a cell-autonomous manner, thus presenting a new target for the control of inflammation in metabolic inflammatory disorders. While CD68 is generally considered a selective marker for myeloid cells, various studies have reported that the expression of CD68 was not restricted to the macrophage lineage (45). Therefore, although CD68 expression in nonmyeloid cells, including fibroblasts, was detected at a variable but lower level compared with monocytes and macrophages, we cannot rule out a minor contribution of these cells to the phenotype observed in MacT3 mice. Moreover, this approach limited the opportunity to identify the circumstances regulating physiological TIMP3 release in adipose tissue and liver. In conclusion, to our knowledge our study is the first to describe a protective effect of TIMP3 on insulin resistance and NAFLD, thus providing the conceptual basis for further exploitation of a TIMP3-based therapy for metabolic disorders.

ACKNOWLEDGMENTS

This study was supported by the following grants: Telethon GGP08065, Fondazione Roma 2008, Juvenile Diabetes Research Foundation Regular Research 1-2007-665, FP7-Health-241913 FLORINASH and EURHYTHDIA, and Ministry of Health RF 2007 (all to M.F.).

No potential conflicts of interest relevant to this article were reported.

R.M. performed experiments, analyzed data, drafted the manuscript, and wrote the final version of the manuscript. V.C., A.M., P.G., and V.M. performed experiments. S.M. researched data and reviewed and edited the manuscript. M.L.H. performed experiments, analyzed data, and drafted the manuscript. A.U. analyzed data. D.L. and P.S. contributed to the discussion and reviewed and edited the manuscript. O.S. performed experiments and analyzed data. G.P. and R.L. contributed to the discussion and reviewed and edited the manuscript. M.F. performed experiments,

analyzed data, drafted the manuscript, wrote the final version of the manuscript, conceived the study, and is the guarantor of this work and, as such, had full access to all the data in the study and takes responsibility for the integrity of the data and the accuracy of the data analysis.

REFERENCES

1. Caldwell SH, Oelsner DH, Iezzoni JC, Hespenheide EE, Battle EH, Driscoll CJ. Cryptogenic cirrhosis: clinical characterization and risk factors for underlying disease. Hepatology 1999;29:664–669
2. Poonawala A, Nair SP, Thuluvath PJ. Prevalence of obesity and diabetes in patients with cryptogenic cirrhosis: a case-control study. Hepatology 2000; 32:689–692
3. Hanley AJ, Williams K, Festa A, et al.; insulin resistance atherosclerosis study. Elevations in markers of liver injury and risk of type 2 diabetes: the insulin resistance atherosclerosis study. Diabetes 2004;53:2623–2632
4. Tilg H, Hotamisligil GS. Nonalcoholic fatty liver disease: cytokine-adipokine interplay and regulation of insulin resistance. Gastroenterology 2006; 131:934–945
5. Pickup JC. Inflammation and activated innate immunity in the pathogenesis of type 2 diabetes. Diabetes Care 2004;27:813–823
6. Schenk S, Saberi M, Olefsky JM. Insulin sensitivity: modulation by nutrients and inflammation. J Clin Invest 2008;118:2992–3002
7. Uysal KT, Wiesbrock SM, Marino MW, Hotamisligil GS. Protection from obesity-induced insulin resistance in mice lacking TNF-alpha function. Nature 1997;389:610–614
8. Cai D, Yuan M, Frantz DF, et al. Local and systemic insulin resistance resulting from hepatic activation of IKK-beta and NF-kappaB. Nat Med 2005;11:183–190
9. Winer S, Chan Y, Paltser G, et al. Normalization of obesity-associated insulin resistance through immunotherapy. Nat Med 2009;15:921–929
10. Federici M, Hribal ML, Menghini R, et al. Timp3 deficiency in insulin receptor-haploinsufficient mice promotes diabetes and vascular inflammation via increased TNF-alpha. J Clin Invest 2005;115:3494–3505
11. Murphy G, Murthy A, Khokha R. Clipping, shedding and RIPping keep immunity on cue. Trends Immunol 2008;29:75–82
12. Davis GE, Senger DR. Extracellular matrix mediates a molecular balance between vascular morphogenesis and regression. Curr Opin Hematol 2008; 15:197–203
13. Menghini R, Menini S, Amoruso R, et al. Tissue inhibitor of metalloproteinase 3 deficiency causes hepatic steatosis and adipose tissue inflammation in mice. Gastroenterology 2009;136:663–672, e4
14. Fiorentino L, Vivanti A, Cavalera M, et al. Increased tumor necrosis factor alpha-converting enzyme activity induces insulin resistance and hepatosteatosis in mice. Hepatology 2010;51:103–110
15. Monroy A, Kamath S, Chavez AO, et al. Impaired regulation of the TNF-alpha converting enzyme/tissue inhibitor of metalloproteinase 3 proteolytic system in skeletal muscle of obese type 2 diabetic patients: a new mechanism of insulin resistance in humans. Diabetologia 2009;52:2169–2181
16. Cardellini M, Menghini R, Martelli E, et al. TIMP3 is reduced in atherosclerotic plaques from subjects with type 2 diabetes and increased by SirT1. Diabetes 2009;58:2396–2401
17. Ewens KG, George RA, Sharma K, Ziyadeh FN, Spielman RS. Assessment of 115 candidate genes for diabetic nephropathy by transmission/disequilibrium test. Diabetes 2005;54:3305–3318
18. Barth JL, Yu Y, Song W, et al. Oxidised, glycated LDL selectively influences tissue inhibitor of metalloproteinase-3 gene expression and protein production in human retinal capillary pericytes. Diabetologia 2007;50:2200–2208
19. Gelling RW, Yan W, Al-Noori S, et al. Deficiency of TNFalpha converting enzyme (TACE/ADAM17) causes a lean, hypermetabolic phenotype in mice. Endocrinology 2008;149:6053–6064
20. Serino M, Menghini R, Fiorentino L, et al. Mice heterozygous for tumor necrosis factor-alpha converting enzyme are protected from obesity-induced insulin resistance and diabetes. Diabetes 2007;56:2541–2546
21. Chavey C, Mari B, Monthouel MN, et al. Matrix metalloproteinases are differentially expressed in adipose tissue during obesity and modulate adipocyte differentiation. J Biol Chem 2003;278:11888–11896
22. Lang R, Rutschman RL, Greaves DR, Murray PJ. Autocrine deactivation of macrophages in transgenic mice constitutively overexpressing IL-10 under control of the human CD68 promoter. J Immunol 2002;168:3402–3411
23. Hogan B, Beddington R, Costantini F, Lacy E. *Manipulating the Mouse Embryo*. 2nd ed. Cold Spring Harbor, NY, Cold Spring Harbor Laboratory Press, 1994
24. Casagrande V, Menghini R, Menini S, et al. Overexpression of tissue inhibitor of metalloproteinase 3 in macrophages reduces atherosclerosis in low-density lipoprotein receptor knockout mice. Arterioscler Thromb Vasc Biol 2012;32:74–81
25. Menghini R, Marchetti V, Cardellini M, et al. Phosphorylation of GATA2 by Akt increases adipose tissue differentiation and reduces adipose tissue-related inflammation: a novel pathway linking obesity to atherosclerosis. Circulation 2005;111:1946–1953
26. Smedsrød B, Pertoft H. Preparation of pure hepatocytes and reticuloendothelial cells in high yield from a single rat liver by means of Percoll centrifugation and selective adherence. J Leukoc Biol 1985;38:213–230
27. Tilg H, Moschen AR. Evolution of inflammation in nonalcoholic fatty liver disease: the multiple parallel hits hypothesis. Hepatology 2010;52:1836–1846
28. Varlamov O, Somwar R, Cornea A, Kievit P, Grove KL, Roberts CT Jr. Single-cell analysis of insulin-regulated fatty acid uptake in adipocytes. Am J Physiol Endocrinol Metab 2010;299:E486–E496
29. Adachi M, Brenner DA. High molecular weight adiponectin inhibits proliferation of hepatic stellate cells via activation of adenosine monophosphate-activated protein kinase. Hepatology 2008;47:677–685
30. Marra F, Bertolani C. Adipokines in liver diseases. Hepatology 2009;50: 957–969
31. Saunders WB, Bohnsack BL, Faske JB, et al. Coregulation of vascular tube stabilization by endothelial cell TIMP-2 and pericyte TIMP-3. J Cell Biol 2006;175:179–191
32. Rupnick MA, Panigrahy D, Zhang CY, et al. Adipose tissue mass can be regulated through the vasculature. Proc Natl Acad Sci USA 2002;99:10730–10735
33. Bernot D, Barruet E, Poggi M, Bonardo B, Alessi MC, Peiretti F. Down-regulation of tissue inhibitor of metalloproteinase-3 (TIMP-3) expression is necessary for adipocyte differentiation. J Biol Chem 2010;285:6508–6514
34. Wang Y, Sul HS. Ectodomain shedding of preadipocyte factor 1 (Pref-1) by tumor necrosis factor alpha converting enzyme (TACE) and inhibition of adipocyte differentiation. Mol Cell Biol 2006;26:5421–5435
35. Österreicher CH, Penz-Österreicher M, Grivennikov SI, et al. Fibroblast-specific protein 1 identifies an inflammatory subpopulation of macrophages in the liver. Proc Natl Acad Sci USA 2011;108:308–313
36. Murthy A, Defamie V, Smookler DS, et al. Ectodomain shedding of EGFR ligands and TNFR1 dictates hepatocyte apoptosis during fulminant hepatitis in mice. J Clin Invest 2010;120:2731–2744
37. Zou C, Ma J, Wang X, et al. Lack of Fas antagonism by Met in human fatty liver disease. Nat Med 2007;13:1078–1085
38. Foveau B, Ancot F, Leroy C, et al. Down-regulation of the met receptor tyrosine kinase by presenilin-dependent regulated intramembrane proteolysis. Mol Biol Cell 2009;20:2495–2507
39. Gerin I, Louis GW, Zhang X, et al. Hyperphagia and obesity in female mice lacking tissue inhibitor of metalloproteinase-1. Endocrinology 2009;150: 1697–1704
40. Jiang H, Zhu H, Chen X, et al. TIMP-1 transgenic mice recover from diabetes induced by multiple low-dose streptozotocin. Diabetes 2007;56:49–56
41. Boden G, Song W, Pashko L, Kresge K. In vivo effects of insulin and free fatty acids on matrix metalloproteinases in rat aorta. Diabetes 2008;57:476–483
42. Duval C, Thissen U, Keshtkar S, et al. Adipose tissue dysfunction signals progression of hepatic steatosis towards nonalcoholic steatohepatitis in C57BL/6 mice. Diabetes 2010;59:3181–3191
43. Jaworski DM, Sideleva O, Stradecki HM, et al. Sexually dimorphic diet-induced insulin resistance in obese tissue inhibitor of metalloproteinase-2 (TIMP-2)-deficient mice. Endocrinology 2011;152:1300–1313
44. Demeulemeester D, Scroyen I, Voros G, et al. Overexpression of tissue inhibitor of matrix metalloproteinases-1 (TIMP-1) in mice does not affect adipogenesis or adipose tissue development. Thromb Haemost 2006;95:1019–1024
45. Kunz-Schughart LA, Weber A, Rehli M, et al. The "classical" macrophage marker CD68 is strongly expressed in primary human fibroblasts. Verh Dtsch Ges Pathol 2003;87:215–223 [in German]